JOURNAL OF APPLIED ELECTROCHEMISTRY **27** (1997) 243–253

The manganese dioxide electrode Part XIII: An FTIR study of H-insertion into EMD

J. FITZPATRICK, L. A. H. MACLEAN, D. A. J. SWINKELS*, F. L. TYE

Energy Technology Centre, Middlesex University, Bounds Green Road, London N11 2NQ, Great Britain

Received 26 March 1996; revised 10 June 1996

Two battery active γ-manganese dioxides, coded R2 and IBA 19, with ~100% microtwinning and ~40% de Wolff disorder were inserted with H by chemical methods in a nonaqueous environment. Compounds with compositions varying from the starting material to the fully H-inserted material were prepared and investigated by FTIR spectroscopy. Both series of compounds exhibited little change in their FTIR patterns until an H-insertion level expressed by s in MnO_nH_s of $s = 0.63$ (R2) and $s = 0.55$ (IBA 19) consistent with the idea that H^+ and e^- are mobile in the structure and present as independent thermodynamic components in an ideal solid solution. Beyond this level H location occurred as evidenced by a sharp change in integrated areas of regions of the spectra associated with O—H bond formation. Simultaneously a change in the position of one of the vibrations associated with that of the $[MnO_6]$ octahedra occurred. The assignment of bands in the spectra is discussed and evidence presented using a modified cusum procedure which supports the proposal that a de-microtwinning of the structure occurs as H begins to locate and the structure expands anisotropically.

1. Introduction

The type of EMD (Electrodeposited Manganese Dioxide) studied in this work has been utilized commercially in primary Leclanché and alkaline manganese batteries. Such EMD is a member of the imperfectly crystalline γ-manganese dioxides, which are materials related to ramsdellite and pyrolusite by various proportions of two types of random structural disorder [1], de Wolff disorder and microtwinning. H–insertion, which occurs at the cathode during discharge, has been the subject of many previous investigations [2–12]. These investigations have established that a solid solution is formed with H-insertion. The principal evidence comes from the continuous shift of XRD lines and the progressive decrease of electrode potential with composition. Recently, by application of statistical thermodynamic principles, the dependence of the electrode potential versus composition has been used to provide strong evidence that inserted H^+ and e^- are present, at least up to 40% H-insertion level, as independent thermodynamic components in an ideal solid solution [13]. A statistical random planar site model was developed which provided insight into the causes of deviations from ideality. Stable microdomains of the end product were predicted for high insertion levels due to the clustering of H^+ e^- pairs on adjacent sites. These stabilized regions contain immobile H in contrast to the surrounding solid solution which allows independent mobility of H^+ and e^-. New XRD lines characteristic of the end product which appear at deep insertion levels have already provided evidence for the existence of such microdomains [11]. It has been suggested that the origin of these new lines result from anisotropic expansion in the ***b*** orthorhombic direction which leads to a demicrotwinning of the structure [14]. In this work FTIR (Fourier Transform Infrared) spectroscopy has been used to probe the structure of chemically prepared H-insertion compounds and to provide further insight into the nature of H in such compounds.

2. Materials

Two commercially available EMDs have been studied. One of these, coded R2, has been extensively characterized as to its physicochemical properties in previous works. Recently the structural parameters have also been determined [14]. The other IBA (International Battery Association) sample 19 is a material having an indistinguishable XRD pattern to R2 [15]. Known common physicochemical parameters are listed for comparison in Table 1.

3. Experimental details

H was inserted into the EMDs by chemical insertion techniques. The object was to produce a range of compounds reflecting the fundamental solid state reaction given by Equation 1.

$$MnO_n + sH^+ + se \rightarrow MnO_nH_s \qquad (1)$$

In this notation the starting nonstoichiometric compound is represented as an oxygen deficient material (i.e., as MnO_n) rather than as $MnOOH_r$ (as in pre-

*Address: Department of Chemistry, University of Newcastle, Callagham, 2308, Australia.

0021-891X

Table 1. Comparison of physicochemical properties of EMDs R2 and IBA 19

Property	*Material R2*	*Reference*	*Material IBA 19*	*Reference*
Stoichiometry	$MnO_{1.945}$	[11]	$MnO_{1.959}$	this work
%Microtwinning	~100	[14]	~100	this work
% de Wolff disorder	41	[14]	37	this work
Combined water	4.33%	[16]	3.22%	this work
Surface area ($m^2\ g^{-1}$)	38	[17]	34	[18]
Mean Particle† size (μm)	40.3	this work	49.8	[19]

† Calculated from the mass fraction distribution using $(\sum x d\phi)/(\sum d\phi)$, where x is the average particle size and $d\phi$ the percentage in the given particle size range [20].

vious works) which implies (for an unknown reason) that residual H of an amount sufficient to cause the same lowering of manganese valence is present in the starting material. Postulating that the material is oxygen deficient with $n < 2$ (for γ-manganese dioxide) has been argued to be preferable to the assumption of inactive H otherwise required in models of the electrode potential [13].

Combinations of acetone, xylene and cinnamyl alcohol in xylene were used to effect a slow homogeneous H insertion into material R2 at ambient temperature as previously described [11]. In the case of IBA 19, 1-propanol under reflux conditions was used to produce H-insertion which has also been described elsewhere [14]. Considerable effort was applied to ensure that non-aqueous conditions prevailed during H insertion in order to avoid complicating reactions involving soluble manganese. Nevertheless such reactions were not completely avoided possibly because of the slight solubility of ionic manganese species in the above mentioned organic solvents.

The level of H-insertion was determined by the double potentiometric titration method introduced by Vetter and Jeager which enables determination of the 'available oxygen' and total manganese to be made on a single sample [21].

Samples for FTIR spectroscopy were prepared by the following procedure. About 3 mg of each sample was mixed with about 450 mg of CsI. Approximately 200 mg of this mixture was used to produce compressed pellets of known weight. The data was recorded on two instruments. H-inserted R2 spectra were recorded on a Nicolet MX-IE FTIR spectrometer to give data of nominal resolution 2 cm^{-1} which were averaged to give spectra in the region 4800–225 cm^{-1}. A reference spectra of CsI was subtracted and the spectra were normalized to 1 mg cm^{-2} using the recorded weights. Further processing of the data was employed to give data at interval of 8 cm^{-1} and this data was finally saved in Lotus spreadsheets. The spectra of H-inserted IBA 19 were recorded on a Perkin Elmer PE 1750 FTIR spectrometer, after similar data processing to that already described data with a resolution of 4 cm^{-1} was saved in the wavenumber range 400–4000 cm^{-1}. Both sets of data were manipulated in spreadsheet form and also imported into the FTIR software program Grams/386 (Galactic Ind. Corp.) which was used for determination of peak positions and deconvolution of overlapping peaks.

4. Results and discussion

4.1. *FTIR spectra of EMD*

It has been established that vibrations of manganese oxides at low wavenumber are generated by the ionic framework while those at higher wavenumbers are due to hydrous components of the oxides [22]. Although 1400 cm^{-1} has been used as the wavenumber separating these two regions [22] it is clear in the present work that 800 cm^{-1} is a more correct choice. Figure 1 compares the FTIR spectra of R2 and IBA 19. That the spectra are practically identical shows that not only the crystallographic structure but also the local vibrational environments are very similar for the two materials. In the region below 800 cm^{-1} a broad band centred at about 580 cm^{-1} with a number of shoulders at lower and higher wavenumber is apparent. This region was resolved into six overlapping bands using the decomposition computer program. The second region shows a broad rising band populated with a number of small features at frequencies of 1100, 1500–1580 and 3250 cm^{-1}. Ideally, to obtain optimum quality i.r. spectra of inorganic compounds, the particle size should be less than the shortest wavelength investigated [23]. At a wavenumber of 4000 cm^{-1} this corresponds to a particle size of 2.5 μm whereas the mean particle sizes quoted in Table 1 are 15 to 20 times greater than this. This means that the 'broad rising band' is probably a background effect caused by scattering from the large particle sizes. If background scattering is taken into account the trough at 800 cm^{-1} must arise from a negative band which is probably due to the Christiansen effect [23, 24].

Assignment of the bands to specific vibrations has not yet been carried out for EMD or indeed any γ-manganese dioxide. Assignments are in general difficult to carry out for at least three reasons. (a) It is well known that the size and shape of particles affects the number and position of bands observed in i.r. spectra of inorganic compounds [23]. (Such variations have been observed and explained [25] in terms of different particle morphologies for example in TiO_2 and SnO_2 (rutile structure)). (b) The crystal structure of γ-manganese dioxides consists of a random planar intergrowth of pyrolusite type domains in a ramsdellite matrix accompanied by a random microtwinning of this structure on the (0 2 1)/(0 6 1) planes and is thus not amenable to any analysis procedure which requires a perfect crystalline structure. (c) A normal coordinate analysis has only been carried out for one of the crystalline structures related to the structure of γ-manganese dioxide (i.e., rutile [26], which has the same structure as pyrolusite). An analysis of the

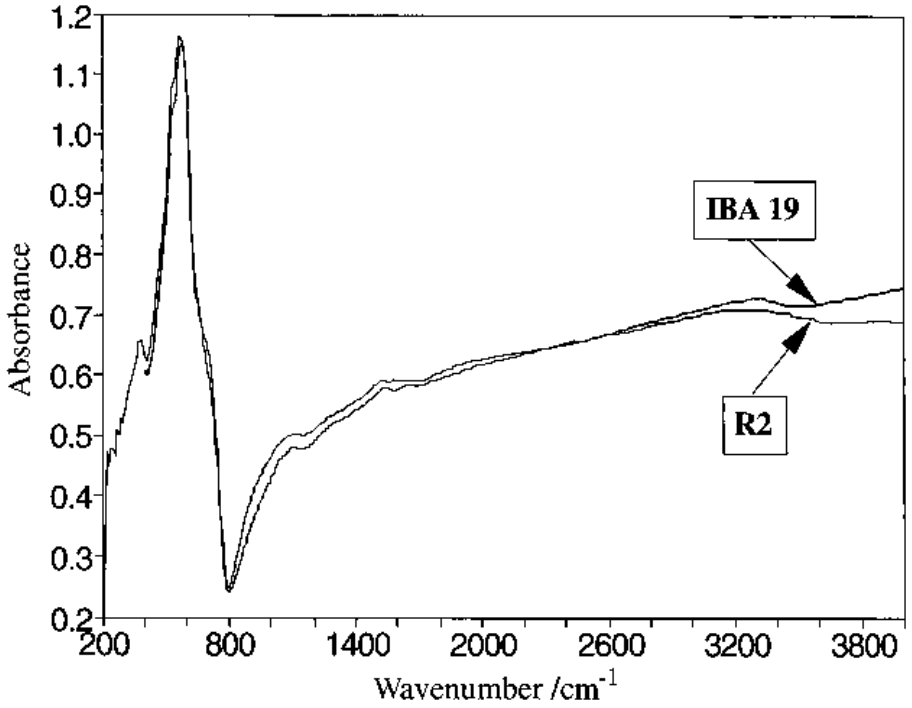

Fig. 1. Comparison of the FTIR spectra of R2 and IBA 19. (The spectra of R2 was multiplied by two for comparison purposes.)

ramsdellite spectra in terms of assignment of bands has not, to the authors knowledge, received any attention in the literature.

In the case of the H-inserted counterparts of γ-manganese dioxide, however, a partial band assignment was made by analogy with α-FeOOH (goethite) which is isomorphous with α-MnOOH, the naturally occurring fully H-inserted counterpart of ramsdellite.

4.2. *FTIR spectra of fully H-inserted EMD*

Figure 2 compares the fully H-inserted spectra of EMD (R2 and IBA no. 19 with the band positions of groutite and manganite (from Appendix A of [22]). After H-insertion the crystal structure is now thought to be that of a demicrotwinned δ-MnOOH [14]. δ-MnOOH being the analogous random inter-

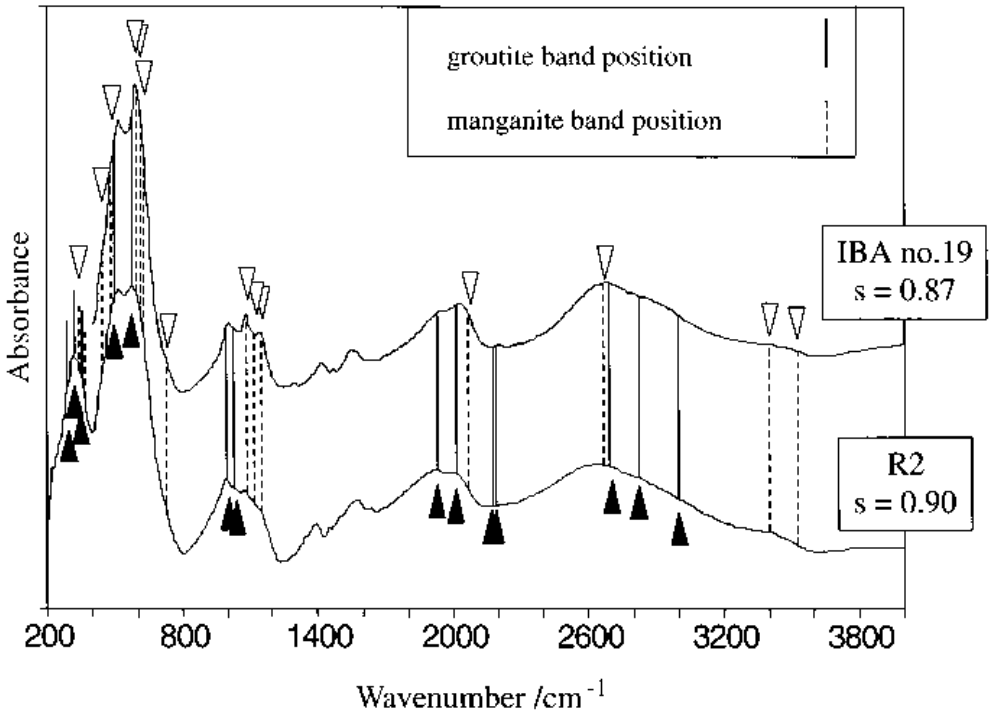

Fig. 2. Comparison of the FTIR spectra of H-inserted EMD with the band positions of groutite and manganite from [22]. (The spectra of H-inserted R2 was multiplied by two).

growth structure to the ramsdellite/pyrolusite intergrowth of the host matrix but this time based on the crystal structures of groutite and manganite. The close resemblance of groutite and manganite structures respectively to those of ramsdellite and pyrolusite makes this possible [14]. Thus if the host material has approximately 40% pyrolusite slabs (Table 1) then the H-inserted counterpart should have 40% manganite slabs in the groutite framework if no structural reorganization has taken place. Since there are twice as many manganese in a ramsdellite or groutite slab compared to a pyrolusite or manganite slab the fully H-inserted material ought to be dominated by the groutite pattern. Figure 2 is compatible with this supposition and accords with recent X-ray diffraction evidence supporting the claim that δ-MnOOH is the crystal structure of the fully H-inserted material [14].

4.3. *Band assignment for α-FeOOH*

The interpretation of the FTIR spectra of the H-inserted compounds is facilitated by comparison with the spectra from α-FeOOH (goethite) which is isomorphous with groutite. Both α-FeOOH and α-MnOOH crystallize in the space group Pbnm with the diaspore structure (α-AlOOH) [27]. Verdonck *et al.* [28] have performed a normal coordinate analysis of α-FeOOH which successfully accounted for the major features of its i.r. spectra. A simplified 'molecular' approach was used which identified molecular groupings dynamically isolated from the surrounding crystal. The model implies that a certain degree of covalency must be present in the chemical bonds. Evidence for a large proportion of covalency has already been presented for Mn(IV) oxides [29, 30]. The calculation was able to account for the vibrational frequencies of both synthetic α-FeOOH and α-FeOOD. The experimental i.r. spectra presented clearly showed how substitution of deuterium did not affect bands below 790 cm^{-1} but shifted a double band at wavenumbers 795 and 886 cm^{-1} to the lower wavenumbers 580 and 680 cm^{-1}. Similarly a broad band centred at 3140 cm^{-1} was shifted to 2330 wavenumbers. The double band was assigned to the O—H in-plane (δ(OH)) and O—H out of plane (γ(OH)) bending modes and the band at 3140 cm^{-1} to an O—H stretch mode. However a number of other smaller bands occurring in the experimental i.r. patterns at intermediate wavenumbers between those of the O—H bending and stretching modes were not assigned to any fundamental frequencies by the authors. Careful reexamination of the pattern suggests them to be combinations and overtones of the O—H bending modes and overtones of two of the [FeO_6] octahedral frequencies.

The above interpretation is reinforced by spectra obtained from a recent inelastic neutron scattering study of α-FeOOH and γ-FeOOH (lepidocrocite) by Hall *et al.* [31] using a time focused crystal analyzer (TFXA) spectrometer. In this technique the hydrogen atom has a very large scattering cross section so that the signals recorded are dominated by H. The largest signals correspond to those with the greatest displacement of the hydrogen atom. Thus $[FeO]_6$ octahedral vibrations, which also involve some displacement of the H atom, are expected to be weak whereas O—H bending and stretching modes are expected to be strong. In a slightly different approach to the one given above the crystal is simplified as a chain of hydrogen bonded species. The largest vibrations were reasoned to be associated with δ(OH) and γ(OH) bending modes. The experimental TFXA spectra were indeed dominated by two peaks at 887 and 1000 cm^{-1} assigned to δ(OH) and γ(OH) which corresponds reasonably well with the i.r. results given previously. Less intense broad bands at ~1700, 1820 and 1990 cm^{-1} were readily assigned to the overtone and combination bands $2 \times \delta$(OH), δ(OH) + γ(OH) and $2 \times \gamma$(OH). Weaker bands at higher frequencies were thought to be $3 \times \gamma$ (OH) (~2600 cm^{-1}) and possibly the O—H stretch frequency (~3200 cm^{-1}). Thus the interpretation given by Hall *et al.* for the TFXA spectra of α-FeOOH accords with the normal coordinate analysis of the i.r. pattern given by Verdonck *et al.* for the peaks involving O—H bonds.

4.4. *Partial band assignment of H-inserted EMD*

By analogy with α-FeOOH the spectra in Fig. 2 also shown as the last spectrum in the series of progressively H-inserted compounds in Figs 7 and 8 may be interpreted as follows. The peaks below 800 cm^{-1} (peaks A, C and D) are due to [$MnO_3(OH)_3$] fundamental vibrations of an octahedron whereas the vibrations above 800 cm^{-1} are mostly due to O—H vibrations. Specifically the doublet marked F is due to the OH bending vibrations (δ(OH) and γ(OH)). The combination of bands centred at about 1900 and 2600 cm^{-1} (G, H, I) are interpreted as combinations and overtones of the bending frequencies. The weak band at ~3400 cm^{-1} (J) is probably an O—H stretch band connected with small quantities of adsorbed molecular water. The broad nature of the band centred at about 2600 cm^{-1} suggests that other hydrous components such as physio-absorbed and chemi-sorbed water may be contributing to this band, however its strength and the strength of the band at 1900 cm^{-1} also suggests that they are possibly highly shifted fundamental O—H stretch bands reflecting extensive H-bonding in the structure. The bands marked B′ and C′ appear not to have any significance in this interpretation. It has been suggested that these bands are due to residual traces of cinnamyl alcohol absorbed on the surface of the oxyhydroxide [32]. Aside from the fact it is much more likely to be that of the corresponding aldehyde these peaks also appear in H-inserted IBA 19 in which 1-propanol not cinnamyl alcohol was used to effect H-insertion and in other materials where hydrazine suspended in hexane was the reducing agent [34].

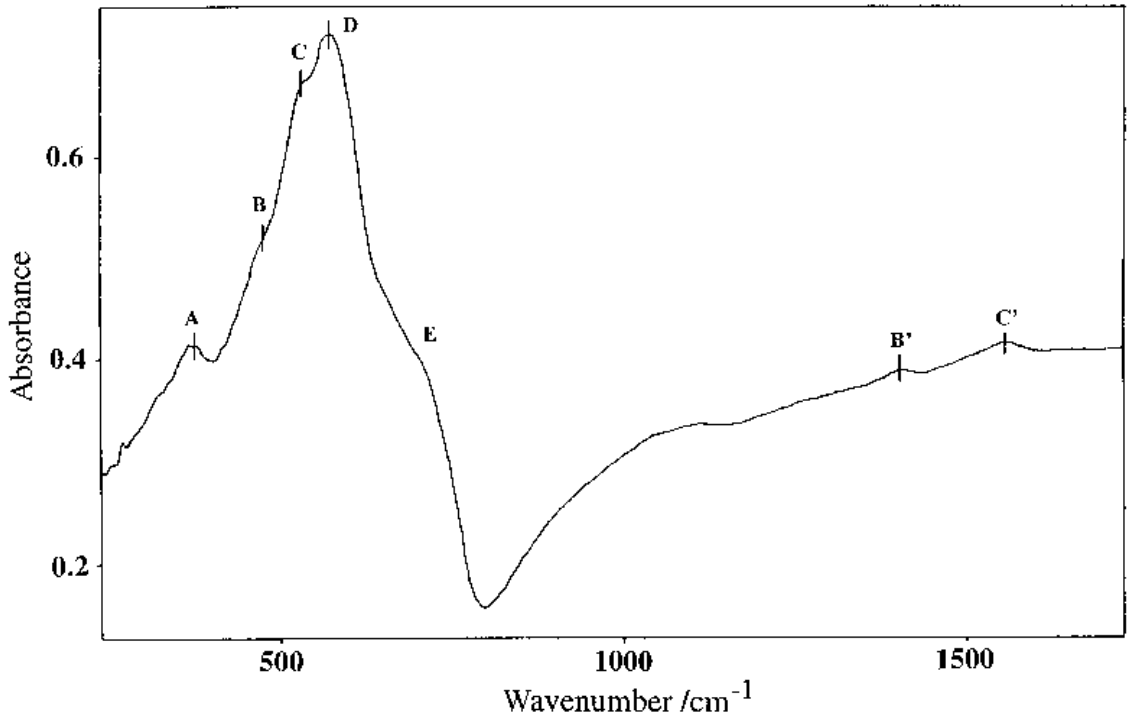

Fig. 3. Demonstration of the existence of two 3rd order overtones in the FTIR spectra of partially H-inserted γ-manganese dioxide ($MnO_{1.945}H_{0.080}$).

Consider Fig. 3 which shows two small peaks in the positions 1404.1 and 1557.6 cm^{-1} for slightly H-inserted R2 ($s = 0.08$). Using the positions of peaks B and C (which were estimated from a visual evaluation) and forming the ratios of B′/B (= 2.94) and C′/C (= 2.93) produces a value close to three for both ratios. There is also some evidence for these peaks in the starting materials though they are extremely weak (see Fig. 1). Peaks B′ and C′ appear more clearly in the first H-inserted samples (R2 and IBA 19) but C′ becomes extremely weak in the R2 H-inserted samples such that it can not be measured in the H-insertion range $s = 0.30$ to 0.83. As may be seen from Fig. 3 it is possible to estimate the positions of B and C by inspection of the pattern. In the case of B, however, this becomes increasingly difficult with H-insertion level due to overlapping of nearby peaks whereas peak C resolves into a clear peak at maximum H-insertion level (see Fig. 7). It was also possible to resolve the overlapping peaks in the region 200–800 cm^{-1} into six component peaks using a mixed gaussian/lorentzian line profile but this yielded no additional information. In the case of IBA 19 peak C was measurable across the whole insertion range. The reason why the behaviour is different has not yet been established. Forming the ratio of C′/C at each insertion level and combining the results of IBA 19 and R2 indicated that the ratio C′/C was close to three over the whole insertion range (Fig. 4). This suggests that C′ is an overtone of C which is a fundamental [MnO_6] octahedral vibration over the whole insertion range. Analogously B′ is also probably an overtone. Theoretically overtones result from anharmonicity of the vibration [33]. They have wavenumbers close to but never exactly that of an integral number of a fundamental vibration. In this case, as may be seen from Fig. 4, it appears that a change in anharmonicity occurs over the H-insertion range, starting from a value less than three and finishing just above three. Both these effects could, however, reflect a bias in the peak measuring procedure for peak C.

The interpretation that O—H bonds are formed on H-insertion has been rejected by Fillaux *et al.* [32, 35] who offers a radical alternative in their INS study of H-inserted EMD and CMD using a TFXA spectrometer. It was concluded by analogy with their in-

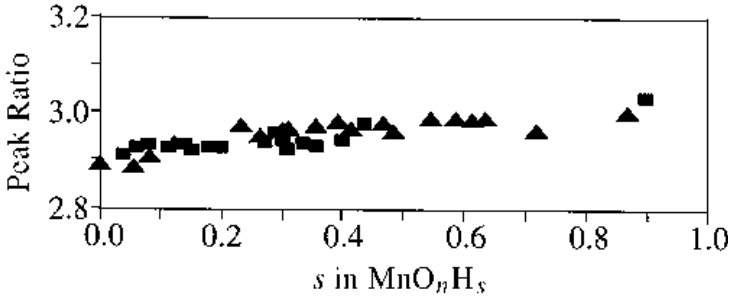

Fig. 4. The peak position ratio of C/C′ measured from the FTIR patterns of H-inserted R2 and IBA 19. Key: (■) R2; (▲) IBA 19.

terpretation of the manganite spectra that γ-OH, δ-OH and ν-OH bands (or combinations thereof) were not observed but rather bands due to protons in octahedra corresponding to $0 \rightarrow 1$, $0 \rightarrow 2$, $0 \rightarrow 3$ transitions of a nearly isotropic oscillator. Bands in the i.r. spectra appeared to support this notion except for the infrared bands at "...~1400 and 1500 cm^{-1} which have no counterpart in INS." [32]. These were attributed to residual traces of cinnamyl alcohol adsorbed on the surface (bands B′ and C′ in this work). In the same paragraph it was further concluded that: "The absence of visible INS bands corresponding to the cinnamic alcohol confirms that it is mostly the surface of the powder which is probed by the infrared while INS is dominated by signals due to protons inserted in the bulk". As may now be appreciated from this work the reason why these bands do not occur in INS is rather because they are overtones of the fundamental [MnO_6] octahedral vibrations which involves relatively small movements of the proton and therefore their INS signal is weak. Thus there is no longer need to invoke surface effects to explain their presence in the infrared.

4.5. *Peak movement of the fundamental [MnO_6] octahedral vibrations with H-insertion level*

Assuming that B′ and C′ are overtones of B and C it is now possible to indicate the variation of four octahedral vibrations with H-insertion level for R2 and three for IBA 19. Figures 5 and 6 indicate the results for R2 and IBA 19, respectively. As may be seen the greatest change occurs for peak A at an H-insertion level $s = 0.63$. The peak position displaces towards lower wavenumber (lower energy) beyond $s = 0.63$.

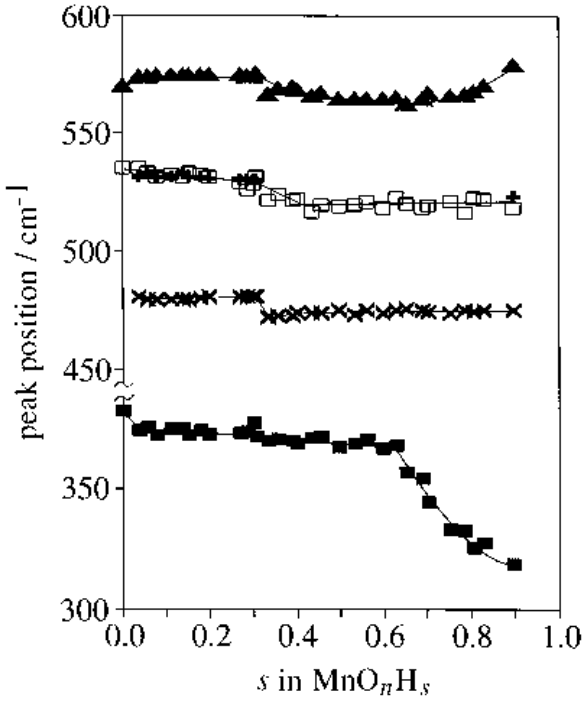

Fig. 5. Variation of R2 FTIR peak positions for 4 fundamental octahedral vibrations with H-insertion level. Key: (■) A; (×) B′/2.93; (+) C′/2.93; (□) C; (▲)D.

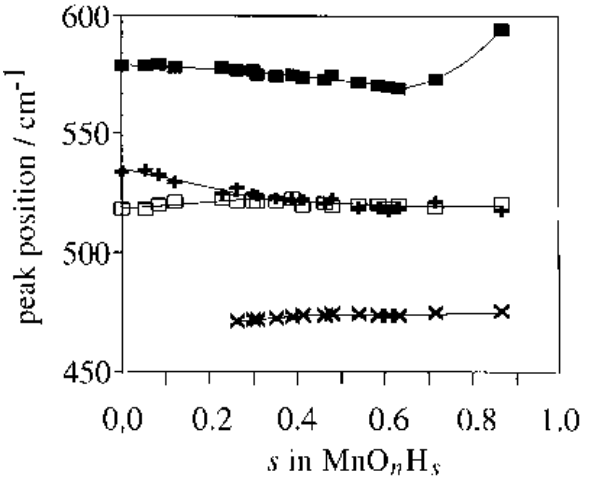

Fig. 6. Variation of IBA 19 FTIR peak positions for three fundamental octahedral vibrations with H-insertion level. Key: (×) B′/2.98; (□) C′/2.98; (+) C; (■) D.

A corresponding increase is observed for peak D at about the same insertion level but no change in behaviour relative to these shifts is observed for peaks C and B. This suggests that peak A is connected with a vibration in the ***b*** orthorhombic direction, which is the predominant direction of dilation for deeply inserted materials [14], whereas B, C and D are associated with vibrations in the ***a*** and ***c*** orthorhombic directions, which show less expansion than that in the ***b*** direction. The behaviour of peaks B, C and D is found to be similar for IBA 19. Additionally there is also some change in behaviour between $s = 0.20$ to $s = 0.30$ particularly for R2.

It is emphasized that no new peaks appear in the spectra below 800 cm^{-1} with H-insertion into R2 and IBA 19, but rather a development of existing features and a shift of peak A.

4.6. *Evidence for H-location in R2 and IBA 19*

In this Section evidence is presented which supports the idea that microdomains of the end product are formed at deep H-insertion levels due to clustering of H^+e^- pairs on adjacent sites as first proposed by Tye and Tye. Figure 7 displays a selection of spectra representing the effect of H-insertion into EMD R2. To detect the point at which O—H bonds begin to form the spectra in region 2 (i.e., 800–4000 cm^{-1}) were sectioned into three regions which captured the expected emergence of the peaks associated with O—H bond formation (ar1, ar2 and ar4 in Fig. 9). A fourth region (labelled ar3) defines the boundaries associated with the overtone peaks. Subtraction of the background delineated by the straight line connecting the boundaries from the integrated area gave the net areas under ar1–4. This was carried out for each H-insertion level. The peak boundaries used are collected in Table 2. The results of this procedure are displayed in Figs 10 and 11. In the case of H-insertion into R2 peaks ar2 and ar4 are almost independent of insertion level until a common sharp breakpoint is

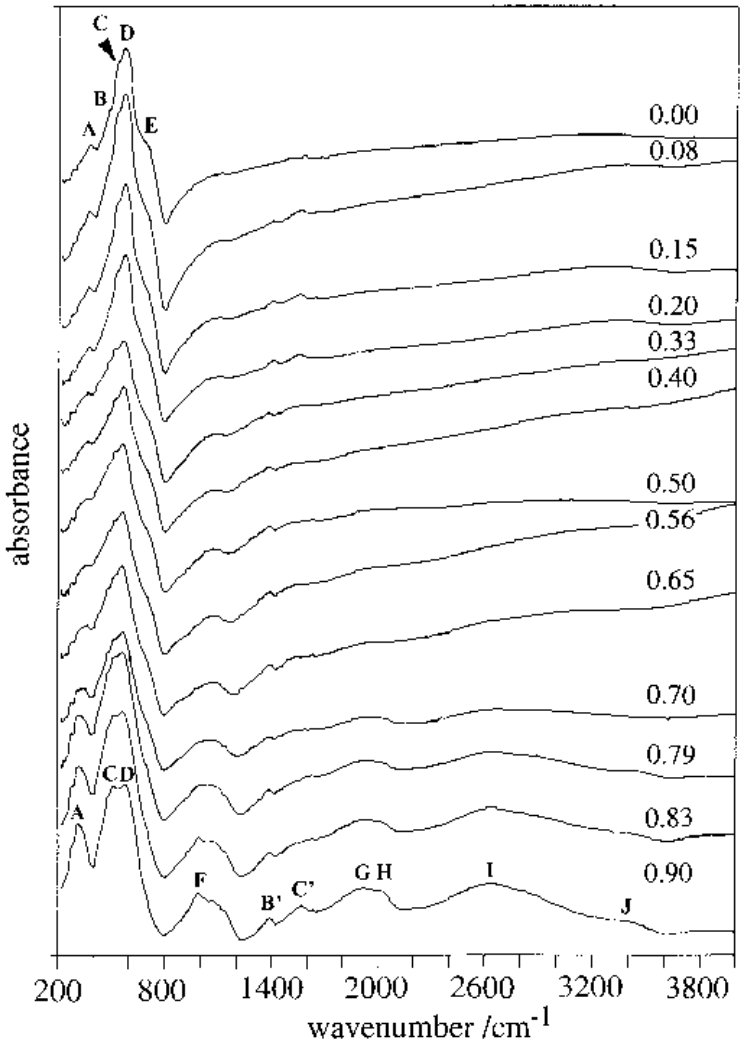

Fig. 7. Selection of stepped FTIR spectra indicating the effect of H-insertion into EMD R2. Peak labels A–E indicate main octahedral vibrations and F–J vibrations associated with O—H bond formation. H-insertion level s in MnO_nH_s is indicated above each spectra.

reached followed by a rapid linear increase in peak area. The breakpoint is at ($s = 0.64$, which corresponds well with the sharp change in position of peak A ($s = 0.63$). A breakpoint also appears to occur for the peak area under ar1, although it is not as clearly defined as in ar2 or ar4. Choosing the high wavenumber boundary for this area to be close to 3600 cm^{-1} so that it includes the broad peak at ~3400 cm^{-1} results in an increase in scatter of the data presumably because this region is affected by O—H stretch vibrations from surface hydroxyls the quantity of which is dependent on the history (especially on the partial vapour pressure of water) of the sample storage conditions. Similar conclusions hold for IBA 19. In this case, however, after the breakpoint a rising curve is observed instead of a straight line. This is attributed to contributions to the peaks from a source other than that of the fundamental H-insertion reaction. As shown in Fig. 2 and Fig. 8 there is clearly a distinct signature of manganite (peaks m_1 and m_2 in fig. 8) in this set of samples which is assumed to be responsible and probably results from a side reaction involving soluble manganese in boiling propanol during H-insertion. The manganese solubility is expected to be less for the room temperature cinnamyl alcohol method of H-insertion. The same reason also explains why the onset of O—H bond formation in this set of samples begins at a slightly lower H-insertion level $s \simeq 0.55$. The absence of any effect of H-insertion below $s = 0.63$ (R2) and $s = 0.55$ (IBA 19) is regarded as strong evidence that O—H bonds are not formed by the inserted H which is present as mobile H^+ ions. Confirmation that area ar3 is associated with overtones of the fundamental octahedral vibrations is the absence of a breakpoint associated with the formation of O—H bonds (Fig. 12.).

Table 2. Peak boundaries used in the determination of the areas ar1–4

Peak label	*Boundaries* /cm^{-1}
ar1	2248–3200
ar2	1752–2152
ar3	1300–1672
ar4	856–1224

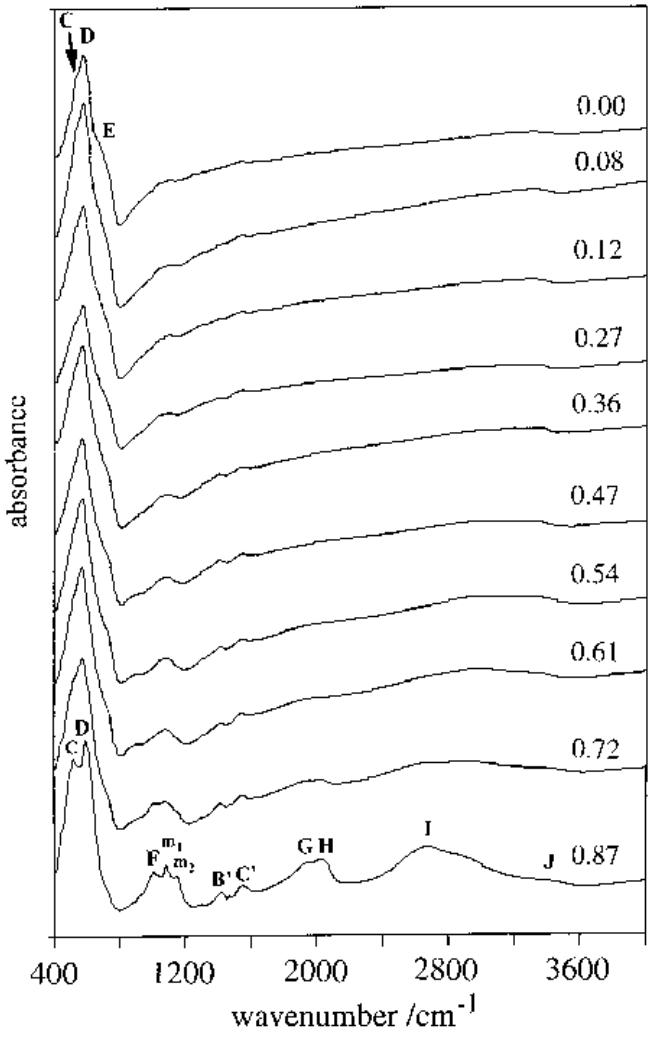

Fig. 8. Selection of stepped FTIR spectra indicating the effect of H-insertion into EMD IBA 19. Peak labels C, D, E indicate main octahedral vibrations and F–J vibrations associated with O—H bond formation. m_1 and m_2 mark manganite peaks. H-insertion level s in MnO_nH_s is indicated above each spectra.

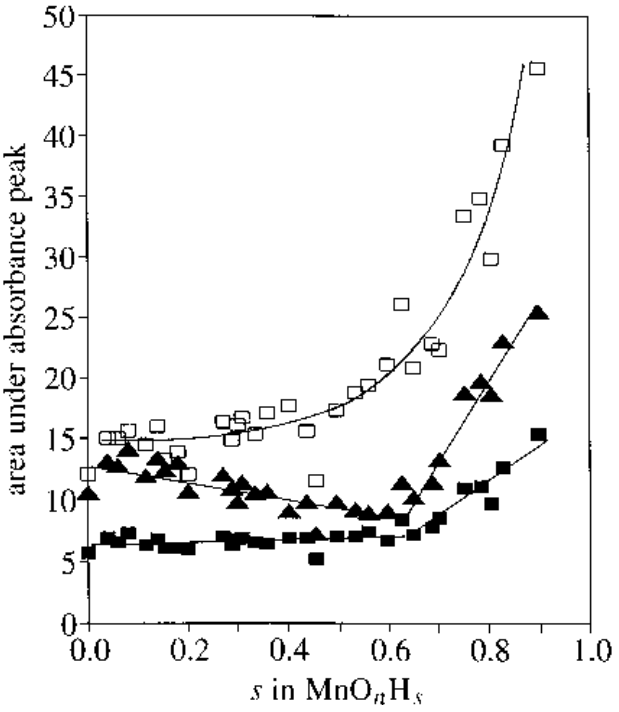

Fig. 10. Integrated areas ar1–4 (as defined in Fig. 9) for H-insertion into R2. Key: (□) ar1; (■) ar2; (▲) ar4.

4.7. *Evidence for demicrotwinning*

It has been concluded recently that a demicrotwinning of the structure occurs for deep H-insertion levels most probably as a result of anisotropic expansion of the structure [14]. As mentioned earlier, a large rising background is observed above 800 cm^{-1} in the spectra as a result of scattering from the large particle sizes in the materials. Each particle consists of a large number of densely packed crystallites. If a

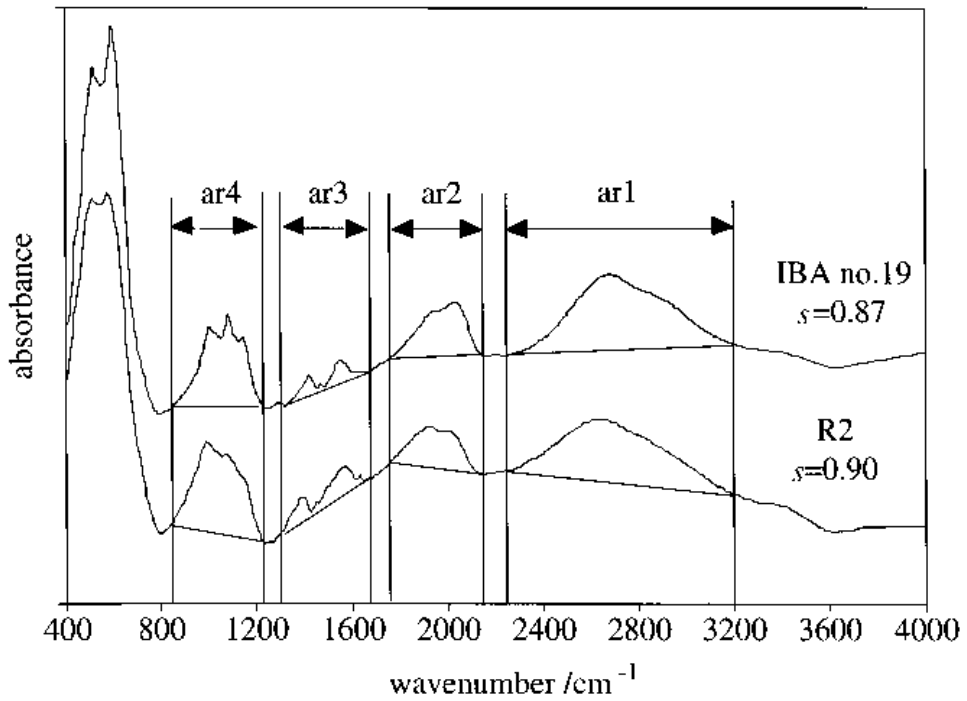

Fig. 9. Definition of area boundaries of regions ar1–ar4.

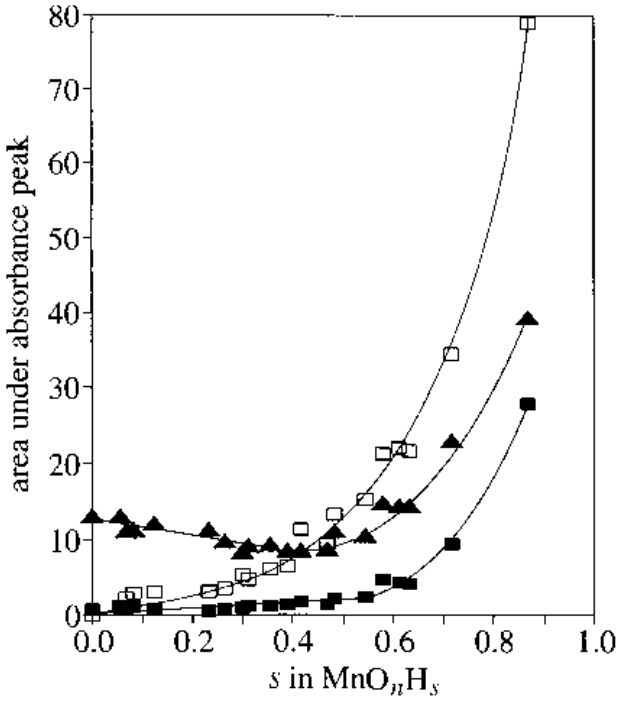

Fig. 11. Integrated areas ar1–4 (as defined in Fig. 9) for H-insertion into IBA 19. Key: (□) ar1; (■) ar2; (▲) ar4.

demicrotwinning of the structure took place this could break up the crystallites in the particle and such behaviour might manifest itself as a large change in the infrared background of the material. To investigate this proposal the absorbance versus insertion level at a wavenumber not contributed to by peaks in the spectra was chosen (3800 cm^{-1}). Using a modified cusum (cumulative sum) procedure (see Appendix) cusum plots were constructed which show a large change in behaviour at about $s = 0.68$ for R2(Fig. 13) and $s = 0.60$ for IBA 19 (Fig. 14). The direction of the cusum plot beyond the breakpoints is in that of a decreasing rate of absorbance against insertion level. Choosing the wavenumber to be in the region of a peak (say, at 1000 cm^{-1}) produces plots with opposite characteristics i.e. the change is in the direction of increasing rate of absorbance versus insertion level. The conclusion is that the background shows little change until the higher levels of H-insertion, $s = 0.70$ for R2 and $s = 0.60$ for IBA 19 when the structure has demicrotwinned and the background drops dramatically.

5. Summary and conclusions

The spectra of fully H-inserted EMD between 200–4000 cm^{-1} divide into two regions as previously proposed. The region below 800 cm^{-1} contains peaks due to fundamental vibrations of $[MnO_3(OH)_3]$ octahedra and the region above 800 cm^{-1} primarily contains peaks due to OH vibrations. O—H bonds, as evidenced by the change in integrated areas ar1, ar2 and ar4 begin to form at insertion levels beyond $s = 0.64$ in R2 and $s = 0.55$ in IBA 19. Up to these insertion levels very little change in the i.r. spectra occurs. Location of H and formation of bonds is accompanied by a rapid change in the position of peak A which is an octahedral vibration. In an XRD study on the same set of samples of R2 Fitzpatrick and Tye observed the appearance of new XRD lines beyond $s = 0.69$. Thus the onset of H location as detected by infrared slightly precedes the insertion level at which structural changes begin to be manifested by XRD.

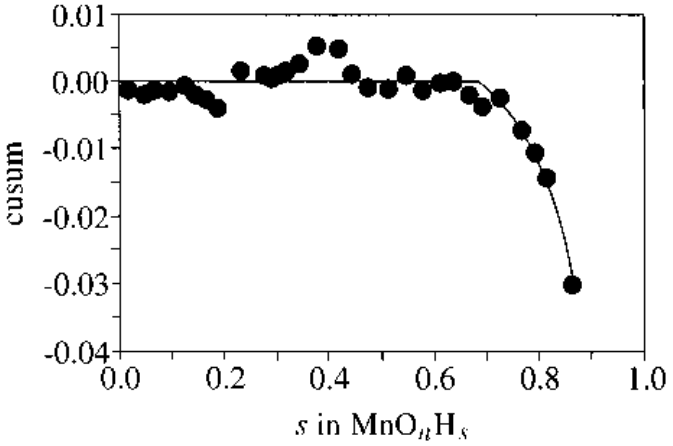

Fig. 13. Modified cusum plot (see Appendix) for absorbance versus H-insertion into R2 at 3802 cm^{-1}.

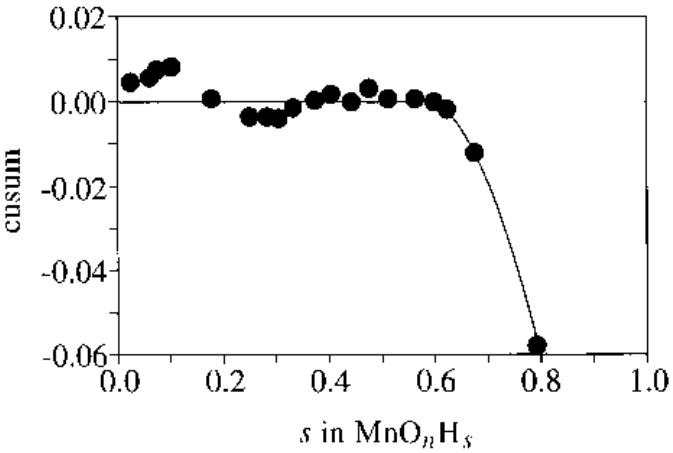

Fig. 14. Modified cusum plot (see Appendix) for absorbance versus H-insertion into IBA 19 at 3800 cm^{-1}.

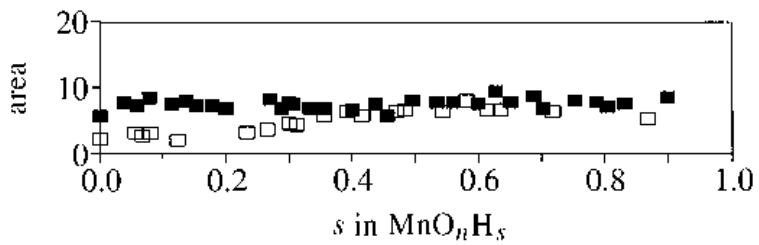

Fig. 12. Integrated area ar3 (as defined in Fig. 9) with H-insertion level for IBA 19 and R2. Key: (■) R2; (□) IBA 19.

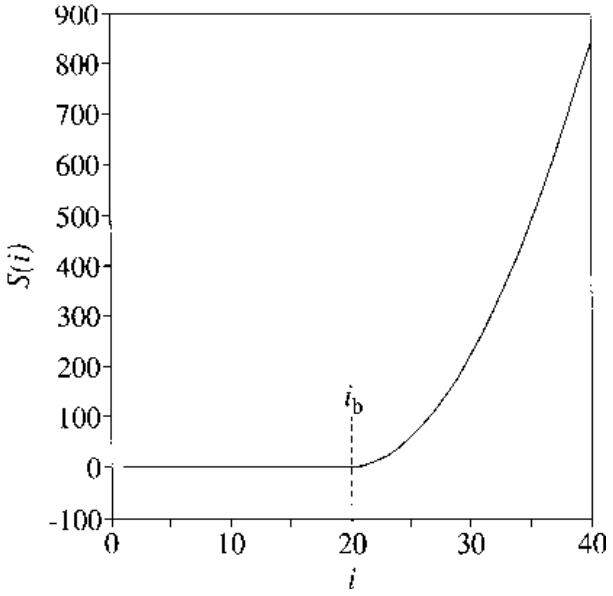

Fig. 15. Modified cusum plot with no error for the case where a change in slope at i_b occurs as given by Equation 4.

The different interpretation proposed by Fillaux *et al.* of the proton bands in INS for H-inserted EMD and CMD may be because manganite was chosen as the compound with which to compare the spectra. As argued previously the H-inserted patterns are expected to be more groutite-like and therefore the analogy with more closely isomorphous α-FeOOH is preferred here. Furthermore the INS spectra were all obtained at 20K the interpretation of which may not apply to the FTIR spectra at room temperature. In either interpretation it is the location of the proton in defined sites beyond a certain H-insertion level which is the important deduction from the present work.

The conclusions are as follows:

(i) H-insertion up to $s = 0.63$ (R2) and $s = 0.55$ (IBA 19) cause little change in the FTIR patterns implying H is mobile in the structure. Beyond these levels the following changes occur: (ii) location of H occurs with accompanying O—H bond formation; (iii) distortion of the $[MnO]_6$ octahedra as evidenced by a rapid change in position of one of the octahedral vibrations; and (iv) a dramatic increase in the rate at which the background decreases with respect to H-insertion in accordance with the idea that a de-microtwinning of the structure takes place.

References

[1] Y. Chabre and J. Pannetier, *Prog. Solid State Chem.***23** (1995) 1.
[2] W. Feitknecht, H. R. Oswald and V. Feitknecht-Steinmann, *Helv. Chimica Acta* **43** (1960) 1947.
[3] J. Brenet, J. Mallessan and A. Grund, *C.R. Acad. Sci.* **242** (1956) 111.
[4] J. P. Gabano, B. Morignat, E. Fialdes, B. Emery and J. F. Laurent, *Z. phys. Chem.* **46**(1965) 359.
[5] W. C. Maskell, J. E. A. Shaw and F. L. Tye, *J. Power Sources* **8**(1982) 113
[6] *Idem, Electrochem.Acta* **28** (1983) 225.
[7] *Idem, ibid.* **28** (1983) 231.
[8] *Idem, ibid.* **26** (1981) 1403.
[9] F. L. Tye, *ibid.* **30** (1985) 17.
[10] S. Atlung and T. Jacobsen, *ibid.* **26** (1981) 1447.
[11] J. Fitzpatrick and F. L. Tye, *J. Appl. Electrochem.* **21** (1991) 130.
[12] R. Giovanoli, K. Bernhard and W. Feitknecht, *Helv. Chim. Acta* **52** (1969) 2333.
[13] F. L. Tye and S. W. Tye, *J. Appl. Electrochem.* **25** (1995) 425.
[14] L. A. H. Maclean and F. L. Tye, accepted for publication in *J. Solid State Chem.*
[15] D. G. Malpas and F. L. Tye, 'Handbook of Manganese Dioxides Battery Grade', (edited by D. Glover B. Schumn and A. Kozawa), International Battery Material Association, Brunswick, OH (1989) p. 177.
[16] D. S. Freeman, P. F. Pelter, F. L. Tye and L. L. Wood, *J. Appl. Electrochem.* **1** (1971) 127
[17] C. St Claire-Smith, J. A. Lee and F. L. Tye, 'Manganese Dioxide Symposium', vol. 1, Cleveland (edited by A. Kozawa and R. J. Brodd), I. C. Sample Office (1975) p. 132
[18] M. Yamashita, M. Ide, H. Takemura, K. Konishi and A. Kozawa, ' Handbook of Manganese Dioxide Battery Grade'*op. cit.* [15], p.259.
[19] *Idem, op.cit.* [15], Appendix, p. 302.
[20] T. Allen, 'Particle Size Measurement', Chapman & Hall, London (1981) p. 127.
[21] K. J. Vetter and N. Yeager. *Electrochim. Acta* **11** (1966) 401.
[22] R. M. Potter and G. R. Rossman, *Amer. Miner.* **64**(1979) 1199.
[23] J. D. Russel, 'Laboratory Methods in Vibrational Spectroscopy' (edited by H. A. Willis, J. H. Van Der Maas, R. G. J. Miller) Ellis Horwood, Chichester, 3rd edn (1989) p. 428.
[24] D. A. J. Swinkels, *op.cit.* [15], p. 253.
[25] M. Ocaña and J. Serna, *Spectrochimica Acta* **47A** (1991) 765.
[26] V. Maroni, *J. Phys. Chem. Solids* **49** (1988) 307.
[27] A. F. Wells, 'Structural Inorganic Chemistry', Clarendon press, Oxford, 5th edn. (1987) p. 639.
[28] L. Verdonck, S. Hoste, F. F. Roelandt and G. P. Van der kelen, *J. Molec. Struct.***79** (1982) 273.
[29] D. M. Sherman, *Amer. Mineral.* **69** (1984) 788.
[30] R. G. Burns and V. M. Burns, 'Manganese Dioxide Electrode Theory and Practice for Electrochemical Application' (edited by B. Schumm, R. L. Middaugh, M. P. Grotheer and J. C. Hunter), The Electrochem. Soc., Pennington, NJ (1985) p. 97.
[31] P. G. Hall, N. S. Clarke and S. C. P. Maynard, *J. Phys. Chem.* **99** (1995) 5666.
[32] F. Fillaux, C. H. Cachet, H. Ouboumour, J. Tomkinson, C. Lévy-Clément and L. T. Yu, *J. Electrochem. Soc.* **140** (1993) 585.
[33] K. Nakamoto, 'Infrared and Raman Spectra of Inorganic and Coordination Compounds', Wiley, New York 3rd edn (1978) p. 9.
[34] L. A. H. MacLean and F. L. Tye, in preparation.
[35] F. Fillaux, H. Ouboumour, C. H. Cachet, J. Tomkinson, C. Lévy-Clément and L. T. Yu, *J. Electrochem. Soc.* **140** (1993) 592.
[36] C. Chatfield, 'Statistics for Technology', Chapman & Hall, London (1985) p. 306.

Appendix

Cusum (cumulative sum) plots are used to detect changes in a quantity defined by an average to a new average value as a result of some change in conditions to the system [36]. The data normally has to be sampled in regular steps, for example a measurement made at the same time every day. Here the procedure was modified to take account of the following differences. Instead of a change to a new average value a change to a new (linear) trend was required. The data was not regularly stepped.

In general for data showing a change in linear slope at the breakpoint

$$y_i = mi + C \tag{2}$$

where y_i is the measured quantity, $i = 1,2,3...$etc., C a chosen constant and m the chosen gradient. To regain a constant at each value of i Equation 2 is solved for C. That is, $C = (y_i - mi)$ and

$$\sum(y_i - mi) - T \tag{3}$$

defines the quantity to be cumulatively summed where T is some target value (which may be adjusted to be equal to C) and m is chosen from a linear regression of the data. The cusum plot is constructed by plotting at each value of i the sum indicated. Unlike a normal cusum, however, the variation of the cusum beyond the breakpoint i_b is not linear. For no error, with $y_i = m_1 + C_1$ for data before the breakpoint and $y_i = m_2 + C_2$ for data beyond the breakpoint, it may be shown that the cusum varies as

$$\begin{aligned} S(i) = &\frac{1}{2}(i^2 + i - i_b^2 - i_b)(m_2 - m) \\ &+ (i - i_b)(C_2 - T) \end{aligned} \tag{4}$$

A plot of the theoretical cusum for the case with $m_1 = 2$, $C_1 = 20$, $m_2 = 6$, $C_2 = -60$ and $i_b = 20$ is shown in Fig. 15.

Equation 3 is valid for regularly stepped data. For nonregularly spaced data (in x) a weighted cusum may be employed, in which case Equation 3 becomes

$$\sum(x_i - x_{i-1})(y_i - mx_i - T) \tag{5}$$

and the data is plotted against $\frac{1}{2}(x_i + x_{i\text{-}1})$.